

31 1. Introduction

32 Gas engines have been increasingly employed as prime movers in transport vehicles [1] and
33 electricity generators [2]. Natural gas (NG) is typically used as the primary fuel for gas engines [3], whilst
34 biogas and pyrolysis gas are also used in countries with abundant biomass or energetic waste resources
35 [4]. Gaseous fuels are usually non-homogeneous mixtures with their composition being highly dependent
36 on the production field (natural gas) or the production process (biomass produced fuels) [5]. In some
37 regions, the pipeline natural gas is mixed with other gaseous fuels or inert gases in order to maintain
38 specific fuel properties [4], which makes the fuel composition greatly varying. The interchangeability
39 between gaseous fuels becomes necessary for gas engines when the fuel composition varies or the main
40 gaseous fuel supply fails. As the fuel composition plays a key role in determining the fuel thermodynamic
41 properties (heating value, specific energy, specific heat, etc.), the fuel composition variation significantly
42 affects the engine performance [6] and emissions [5]. In this respect, the investigation of the fuel
43 interchangeability between gaseous fuels in combustion engines is a topic of great importance.

44 The fuel interchangeability requires that the two gaseous fuels must be nearly identical in terms of
45 their combustion characteristics, efficiency and flame properties. Three main methods have been
46 proposed for estimating the interchangeability of gaseous fuels; in specific, the Weaver method, the
47 American Gas Association (AGA) method and the Wobbe Index (WI). The WI is widely-used in engine
48 applications to assess the interchangeability of gaseous fuels, as the flame indices defined in the Weaver
49 method [7] and the AGA method [8] are more suitable for domestic burners rather than internal
50 combustion engines [9]. Klimstra [10] introduced the WI as a criterion for gaseous fuels
51 interchangeability and concluded that the fuel composition variations appear not to induce noticeable
52 changes to the air-fuel ratio and the combustion velocity when the WI remains constant, whilst the
53 explosion limits and the knock resistance varied to a moderate extent with the fuel composition variations.
54 Karavalakis et al. [11] measured the exhaust emissions of a Cummins 8.3 L natural gas engine operating
55 on seven different fuel gas blends with varying WI and Methane Number (MN). The higher hydrocarbons
56 gaseous fuels were proved to yield higher carbon dioxide (CO₂) and nitrogen oxide (NO_x) emissions,
57 whilst the total hydrocarbons (THC), methane (CH₄), carbon monoxide (CO) and particulate matter (PM)
58 emissions reduced for the fuels with higher hydrocarbons and higher WI. Cardona [12] presented an
59 analysis of the interchangeability between a biogas/propane/hydrogen mixture (50% biogas / 40%
60 propane / 10% hydrogen in volume) and methane in a contoured slot burner, which is based on the WI

61 and the laminar burning velocity, concluding that the variations of these properties between the tested
62 fuels did not exceed 10% of the methane properties; thus enabling the tested mixture to substitute the
63 natural gas. By employing graphical interchangeability methods based on the WI and the combustion
64 potential [13] as well as several multi-index methods [14], it was demonstrated that the plastic pyrolysis
65 gas is a suitable alternative to the natural gas. The previously discussed experimental studies [10-14]
66 combined the WI with other specific indices for accurately evaluating the gaseous fuel interchangeability.
67 However, experimental studies require considerable resources and are costly, therefore they are not handy
68 for a quick and reliable evaluation of the fuels interchangeability.

69 In this respect, a more cost effective method for investigating the fuel interchangeability is by using
70 simulation tools. Engine modelling and simulation enable to obtain a better understanding of the engine
71 components processes characteristics comprehensively during the engine design phase; therefore they
72 can be employed for evaluating the gaseous fuel interchangeability. In general, simulation models for
73 internal combustion engines can be classified as follows (from simpler to more complicated): mean value
74 models, zero-dimensional or one-dimensional models, and multi-dimensional models [15]. The mean
75 value models are usually set up and calibrated by using a large amount of engine test data and are not
76 capable of predicting the in-cylinder parameters variations [16]. The multi-dimensional simulation
77 models (or Computational Fluid Dynamics model) provide the most detailed representation of the in-
78 modelled engine components, and therefore they are appropriate for engine components design studies
79 as well as for obtaining better insight of the involved thermo-physical processes [17]. The zero-
80 dimensional models employ the assumption of uniform variations of the working medium state and
81 concentration within the engine components and is a quite an effective predictive model approach, which
82 is extensively used for engine performance/emissions prediction [18]. For modelling the engine cylinders
83 combustion process, a number of approaches can be used from single zone [19] to multi-zone
84 phenomenological models [20].

85 For the natural gas engines modelling, one of the key objectives is to predict the knocking
86 phenomenon which constrains the further engine thermal efficiency improvement [21]. In this respect, a
87 two-zone zero-dimensional model could be an effective tool for both the engine performance and
88 knocking prediction, as it is capable of characterizing the end-gas temperature with the simplest
89 combustion zone division [22] and it is a compromise between the required model complexity, input data
90 and computational time.

91 Notwithstanding the above, independently of the engine model type is used for the fuel
92 interchangeability investigation, the thermodynamic parameters of the fuel and the in-cylinder gas
93 (heating value, internal energy, enthalpy, specific heat, etc.) must be determined by employing a suitable
94 method. The most frequently employed method is to assume the thermodynamic parameters as constant
95 according to empirical [23] or experimental data [24], or calculate them by the properties and mass
96 fraction assuming that the working medium consists of several basic species [16]. It is reported in [26]
97 that the latter method can achieve higher accuracy as it considers the variation of in-cylinder working
98 medium composition and thermodynamic properties [26]. Ding [27] investigated the thermodynamic
99 properties of the fuel and the in-cylinder working medium in diesel engines by using a first principles
100 calculation method considering the thermodynamic properties functions of the working medium
101 temperature and composition. Neto [28] used the Density Functional Theory (DFT) and the canonical
102 ensemble to investigate the thermodynamic properties of the major molecules compounds at the gaseous
103 phase of fuels like gasoline, ethanol, and gasoline-ethanol mixture, including the internal energy, enthalpy,
104 entropy and Gibbs free energy. Li [29] analysed the average thermodynamic properties of the NG–air
105 mixture, such as the specific heat ratio and the specific heat capacity as functions of the total equivalence
106 ratio by using thermodynamic relations and the ideal gas equation. These studies focused on the in-
107 cylinder thermodynamic parameters of specific liquid or gaseous fuels and cannot be used directly for
108 the interchangeability investigation of gaseous fuels, which requires approaches with great flexibility in
109 the fuel types and compositions.

110 From the proceeding analysis it is deduced that most of the published gaseous fuel interchangeability
111 studies were carried out by employing experimental methods, which are case dependent, time-consuming
112 and involve considerable cost. On the other hand, a two-zone zero-dimensional model can be an effective
113 tool to investigate the fuel interchangeability as well as the knocking performance of internal combustion
114 engines. In addition, most of the numerical methods for thermodynamic properties estimation are limited
115 to specific fuel types, which are not applicable for the model development of an internal combustion
116 engine running on flexible fuels.

117 In this respect, this study aims at extending a zero-dimensional model, which was initially developed
118 for diesel engines, taking into consideration the thermodynamic properties of a number gaseous fuels –in
119 specific natural gas (NG) and hydrogen (H₂)– as well as their combustion products, thus allowing for the
120 development of a model capable of the performance prediction of multi-fuel engines. The model

121 applicability is verified by using experimental data from single-fuel and multi-fuel engines, including a
122 diesel engine, a natural gas spark-ignited (SI) engine, a dual-fuel engine and a tri-fuel engine.
123 Subsequently, the validated model is used to investigate the interchangeability between gaseous fuels
124 with same WI and the influence of inert gases (carbon dioxide and nitrogen) addition on the engine
125 knocking resistance.

126 The novelty of this study is summarised as follows: (a) Extension of a zero-dimensional single-zone
127 model initially developed for diesel engines to a two-zone zero-dimensional model, which is capable of
128 predicting the performance of single-fuel engines and multi-fuel engines; (b) investigation of the engine
129 performance with fuels with the same WI; and (c) Investigation of the influence of the inert gases addition
130 on the engine knocking performance during the fuel interchangeability by employing the developed two-
131 zone knocking model.

132

133 **2. Model Description**

134 This section described the two-zone zero-dimensional model employed in this study in order to
135 investigate the gaseous fuel interchangeability. A number of submodels are used for estimating the
136 combustion heat release rate, the heat transfer from the gas to the engine cylinder walls, the working
137 medium properties, as well as the knocking prediction. The developed model was implemented in the
138 MATLAB/SIMULINK computational environment.

139

140 **2.1 Calculation Principles**

141 The proposed model simulates the closed cycle of one engine cylinder, i.e., the compression,
142 combustion and expansion stage. The specific assumptions for developing the model are outlined as
143 follows.

- 144 1) The working medium inside the cylinder is uniformly distributed, which indicates that its pressure,
145 temperature and concentration are the same throughout the cylinder.
- 146 2) The in-cylinder gas is considered to be ideal but non-perfect. Thus, its thermodynamic properties
147 can be calculated as functions of its temperature and composition.
- 148 3) Dissociation effects are not taken into account. Only the hydrocarbons (HC), sulphur (S) and oxygen
149 (O_2) take part in the reaction and end up with complete combustion products like nitrogen (N_2),
150 oxygen (O_2), argon (Ar), carbon dioxide (CO_2) and water (H_2O).

151 4) Blowby and valves leakage in the engine cylinder are not considered.

152

153 2.1.1 Heat Release

154 Semi-empirical formulas are usually employed to simulate the combustion Heat Release Rate (HRR).
155 Typically, the HRR determining methods include the Triangular Exothermic function, the Polygon-
156 hyperbola function and the Vibe function [30], among which the Vibe function is most widely used. The
157 burnt fuel fraction simulated by a single Vibe function [31] is represented by the following equation:

$$158 \quad x_b = 1 - e^{-a \cdot \tau_v^{m_v+1}} \quad (1)$$

159 where, x_b is the burnt fuel fraction; a is the coefficient related to the combustion efficiency, which is
160 usually set at 6.9078 to maintain a combustion efficiency of 99.9%; τ_v is the normalized combustion time;
161 and m_v is the shape factor.

162 The total heat release in a multi-fuel engine can be obtained by employing several Vibe functions.
163 Generally, two Vibe functions can sufficiently represent the combustion process of a directly injected
164 diesel fuel, which consists of a premixed combustion stage and a diffusion combustion stage. One Vibe
165 function is able to characterize the combustion process of a premixed gas engine as it represents the main
166 characteristics of a premixed combustion. In this study, two parameters, in specific the Total Energy Input
167 (TEI) and Accumulated Heat Release (AHR) are defined to describe the total heat release calculated by
168 using the lower heating value (LHV) and the combustion heat, by employing Eq (2) and Eq (3),
169 respectively. The *Combustion Heat* (u_{comb}) is the specific heat release corresponding to the specific
170 internal energy difference between the combustion reactants and products [27], which will be described
171 in detail in the following section.

$$172 \quad TEI = \sum_{i=1}^N m_i \cdot LHV \quad (2)$$

$$173 \quad AHR = \sum_{i=1}^M \int_{SOC_i}^{EOC_i} m_i \cdot [b_{i,1} \cdot \dot{x}_{b,i,1} + b_{i,2} \cdot \dot{x}_{b,i,2}] \cdot u_{comb,eff,i} dt + \sum_{j=1}^{N-M} \int_{SOC_j}^{EOC_j} m_j \cdot \dot{x}_{b,j} \cdot u_{comb,j} dt \quad (3)$$

174 where, M is the number of the direct injection liquid fuels; N is the number of all the employed fuels;
175 SOC and EOC denote the start and end timing of the fuel combustion. SOC and EOC (for each fuel and
176 Vibe function employed) are estimated by the HRR analysis, which can be either calculated by using the
177 experimentally measured in-cylinder pressure or by using CFD combustion modelling. For per liquid
178 fuel, which requires two Vibe functions to characterise the premixed and diffusion combustion
179 respectively, the $SOCs$ and $EOCs$ are considered the same for both functions in order to simplify the

180 modelling; m is the injected fuel mass of each fuel; $b_{i,1}$ and $b_{i,2}$ are the weigh factors for premixed
181 combustion stage and diffusion combustion stage of direct injection liquid fuels, $b_{i,1} + b_{i,2} = 1$; m_v is the
182 shape factor; $u_{comb,eff,i}$ is the effective combustion heat of each liquid fuel; $u_{comb,j}$ is the combustion heat of
183 each gaseous fuel.

184

185 2.1.2 Heat Transfer

186 The cylinder walls include three parts: the surface of the cylinder head and valves, the surface of the
187 cylinder liner and the top surface of the piston. The temperature of each part of the heat transfer surface
188 is considered to be constant as its variation is small enough to be neglected compared to the in-cylinder
189 gas temperature. The Woschni model [32] is considered for calculating the instantaneous heat transfer
190 coefficient $\alpha_{g \rightarrow w}$ from the in-cylinder gas to walls. The heat transfer between the working medium and
191 the cylinder walls is calculated according to the following equation:

$$192 \quad Q_{\text{loss}} = \sum_1^3 [\alpha_{g \rightarrow w} \cdot (T - T_{\text{wall},i}) \cdot A_{\text{wall},i}] \quad (4)$$

193 where, $\alpha_{g \rightarrow w}$ is the instantaneous heat transfer coefficient from the in-cylinder gas to the walls; $T_{\text{wall},i}$ is
194 the average wall temperature of each surface. $i=1, 2, 3$, which represents the cylinder head and valves,
195 the cylinder liner and the cylinder piston respectively; and $A_{\text{wall},i}$ is the heat transfer surface area.

196

197 2.1.3 Mass Balance and Composition

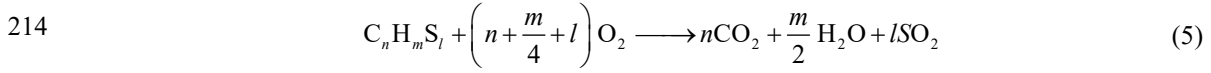
198 In order to estimate the in-cylinder working medium properties in internal combustion engines, the
199 in-cylinder gas is considered as a mixture of several well-defined basic mixtures; in specific, air, gaseous
200 fuel (if any) and stoichiometric gas, whilst all the basic species are considered as ideal but non-perfect.
201 The stoichiometric gas is defined as the complete combustion product of the stoichiometric air-fuel
202 mixture. The constituents of air, gaseous fuel and stoichiometric gas are listed as follows.

- 203 1) Air: Fixed-fraction dry air (N_2 , O_2 , Ar, CO_2) and water vapour (H_2O);
- 204 2) Gaseous fuel: methane (CH_4), ethane (C_2H_6), propane (C_3H_8), n -butane ($n\text{-C}_4\text{H}_{10}$), i -butane ($i\text{-C}_4\text{H}_{10}$), pentane (C_5H_{12}), N_2 , CO_2 (taking natural gas for example);
- 205 3) Stoichiometric gas: N_2 , O_2 , Ar, CO_2 , H_2O .

206

207 For direct injection engines, only the air and the stoichiometric gas need to be considered on the
208 assumption that the injected fuel burns immediately after its injection within the engine cylinder. The

209 mass fractions of the different species in the gaseous fuel and the air can be obtained from the fuel type
 210 and the ambient air humidity respectively, whilst that of the stoichiometric gas needs to be calculated
 211 according to the complete combustion chemical reaction. Assuming that only Hydrocarbons, Sulphur
 212 and Oxygen take part in the combustion reaction, the following equation is used for representing the
 213 combustion.



215 For direct injection engines, the instantaneous mass fraction of the in-cylinder air can be calculated
 216 by using Eq (6). The two terms of the numerator of the right-hand side represent the initial air mass and
 217 accumulated burnt air.

$$218 \quad x = \frac{m_0 \cdot x_0 - \sigma \cdot \int_{SOC}^{EOC} \xi \cdot dt}{m_0} \quad (6)$$

219 where, m_0 is the mass of the in-cylinder mixture at Inlet Valves Close (IVC); x_0 is the initial mass fraction
 220 of fresh air at IVC; σ is stoichiometric air-fuel ratio; ξ is the combustion rate obtained by Vibe function.

221 For premixed combustion engines, the instantaneous mass fraction of air-fuel mixture can be obtained
 222 on the assumption that air and gaseous fuel react at the stoichiometric ratio, according to Eq(7).

$$223 \quad x = \frac{m_0 \cdot x_1 - (1 + \sigma) \cdot \int_{SOC}^{EOC} \xi \cdot dt}{m_0} \quad (7)$$

224 where, x_1 is the initial mass fraction of air-fuel mixture at IVC.

225

226 **2.1.4 In-cylinder gas properties**

227 Assuming that the in-cylinder gas behaves as an ideal but non-perfect gas, the thermodynamic
 228 parameters of each species only depend on the in-cylinder temperature and can be obtained by the power
 229 series equation that varies with the normalized temperature according to Eq (8). Yaws [33] and Borman
 230 [34] obtained the fitting coefficients of various types of gases by using experimental methods.

$$231 \quad c_{p,j} = \sum_{k=1}^l a_{k,j} \theta^{k-1} \quad (8)$$

232 where, a_k is the fitting coefficient of specific heat at constant pressure; θ is normalized temperature, $\theta =$
 233 $(T - T_{shift}) / T_{norm}$; T_{shift} is the shift temperature, $T_{shift}=0$ K; T_{norm} is the normalised reference temperature,
 234 $T_{norm}=1000$ K.

235 The specific heat at constant volume of each species can be calculated by using the gas constant
 236 and the molar mass, according to the following equation.

$$237 \quad c_{v,j} = c_{p,j} - R_j / M_j \quad (9)$$

238 The specific enthalpy and internal energy of each species can be calculated by Eq (10) and Eq (11),
 239 respectively.

$$240 \quad h_j = \int c_p dT + h_j^{ref} = \sum_{k=1}^l \frac{a_{k,j}}{k} \cdot T_{norm} \cdot \theta^k - \sum_{k=1}^l \frac{a_{k,j}}{k} \cdot T_{norm} \cdot \theta_{ref}^k + h_j^{ref} \quad (10)$$

$$241 \quad u_j = \int c_v dT + u_j^{ref} = h_j - R_j \cdot T \quad (11)$$

242 where, h_j^{ref} and u_j^{ref} are specific enthalpy and internal energy at standard conditions; θ_{ref} is normalized
 243 reference temperature.

244 Since each species in air, gaseous fuel and stoichiometric gas are considered ideal but non-perfect
 245 gases, the mixtures behave as ideal but non-perfect as well. Thus, the specific heat, enthalpy and internal
 246 energy of the considered mixtures are functions of the average temperature and their composition. A
 247 power series of the normalized temperature is used to fit these property data for all the species and the
 248 properties of the mixtures can be obtained considering ideal mixtures.

249 The in-cylinder working gas properties, i.e. the specific heat, specific enthalpy and specific internal
 250 energy, can be calculated by species property data and composition fractions according to the following
 251 equation:

$$252 \quad f(x, T) = \sum_l x_l \left(\sum_{j=1}^J x_j f_j(T) \right) \quad (12)$$

253 where, T is the average in-cylinder temperature; $f_j(T)$ is the property data (c_v , h and u) for each basic
 254 species; x_j is the mass fraction of the considered mixture constituents; x_l is the mass fraction of air, gaseous
 255 fuel and stoichiometric gas.

256

257 **2.1.5 Combustion Heat**

258 The *Combustion Heat* (u_{comb}) is introduced for calculating the specific heat release by using the
 259 difference of the specific internal energy between the combustion reactants and products [27]. Compared
 260 to the traditional heating value (HV) determination methods, it considers the influence of instantaneous
 261 temperature on the specific heat release. The combustion heat can be calculated by considering the

262 specific internal energy of the fuel, the air and the stoichiometric gas according to the following equation:

$$263 \quad u_{comb} = u_f + \sigma \cdot u_a - (1 + \sigma) \cdot u_{sg} \quad (13)$$

264 where, u_f , u_a and u_{sg} are the specific internal energy of the fuel, the air and the stoichiometric gas
265 calculated by using the average cylinder temperature and the gas composition.

266 For direct injection engines (including liquid and gaseous fuel engines), the energy change caused
267 by the difference between the injection pressure and the in-cylinder pressure must be taken into
268 consideration. In addition, the evaporation heat must also be included in the energy change for the direct
269 injection engines running on liquid fuels. A direct injection diesel engine is taken as an example to
270 illustrate these two parts of the energy change. The energy change during the process of the diesel fuel
271 injection includes two parts: (a) the kinetic energy increase caused by the velocity variation, and (b) the
272 liquid diesel fuel evaporation. E_f is introduced to represent the sum of these two parts of the energy and
273 it can be calculated by the difference between the specific enthalpy of the liquid diesel and the specific
274 internal energy of the evaporated gaseous diesel [27], according to the following equation:

$$275 \quad \dot{E}_f = \dot{m}_{f,in} \cdot e_f = \dot{m}_{f,in} \cdot (h_{f,liquid}^{in+} - u_{f,gas}) \quad (14)$$

276 where, $h_{f,liquid}^{in+}$ is the specific enthalpy of the liquid diesel fuel; $u_{f,gas}$ is the specific internal energy of the
277 evaporated gaseous diesel fuel; $\dot{m}_{f,in}$ is the injected diesel fuel flow rate. Since the injection rate,
278 evaporation rate and combustion rate are assumed to be the same for the zero-dimensional engine
279 modelling, $\dot{m}_{f,in}$ equals the diesel combustion rate ζ_D .

280 Combining Eq (13), Eq (14) and after some manipulation, Eq (15) is derived, which provides the
281 *Effective Combustion Heat* ($u_{comb,eff}$) for a direct injection engine running on liquid diesel fuel.

$$282 \quad u_{comb,eff,D} = u_{comb,D} + e_f \quad (15) \\ = [u_{f,D} + \sigma_D \cdot u_a - (1 + \sigma_D) \cdot u_{sg,D}] + e_f$$

283 where, $u_{comb,D}$ is the combustion heat of diesel fuel calculated by Eq (13); e_f is the specific energy
284 accounting for the injection pressure difference and the fuel evaporation process.

285

286 **2.1.6 Knocking Prediction**

287 The knocking phenomenon, including conventional knocking and super knocking, is the main
288 obstacle to employ a high compression ratio for improving the thermal efficiency of gas engines. It is

289 generally accepted that the super knocking originates from the pre-ignition in highly boosted gas engines,
 290 especially for fuel direct injection engines in the low-speed high-load operating conditions [35].
 291 According to [36], the conventional knocking is associated with auto-ignition in the unburnt zone after
 292 the combustion start. As the investigated 2135 NG engine is naturally aspirated, only the conventional
 293 knocking phenomenon will be considered in this study. The probability and corresponding crank angle
 294 position of knocking can be determined by Eq (16). According to Livengood and Wu [37], knocking
 295 occurs when the integral of Eq (16) reaches unity.

$$296 \quad I = \int_{t=0}^{t_i} \frac{dt}{\tau} = 1 \quad (16)$$

297 where τ (*in ms*) is the induction time calculated according to Eq (17) as function of the instantaneous
 298 temperature and pressure in unburnt zone; t is the elapsed time from the start of the compression process
 299 of the unburnt zone, and t_i is the time of auto-ignition.

$$300 \quad \tau = 17.68 \left(\frac{\text{ON}}{100} \right)^{3.402} p^{-1.7} \exp \left(\frac{3800}{T_2} \right) \quad (17)$$

301 where ON is the octane number of the fuel; p is absolute pressure in atmosphere, and T_2 is the temperature
 302 in unburnt zone.

303 When the temperature and pressure time variation of the unburnt gas during an individual cycle are
 304 known, Eq (16) and Eq (17) can be used to determine whether auto-ignition occurs before the normally
 305 propagating flame consumes the unburnt gas.

306

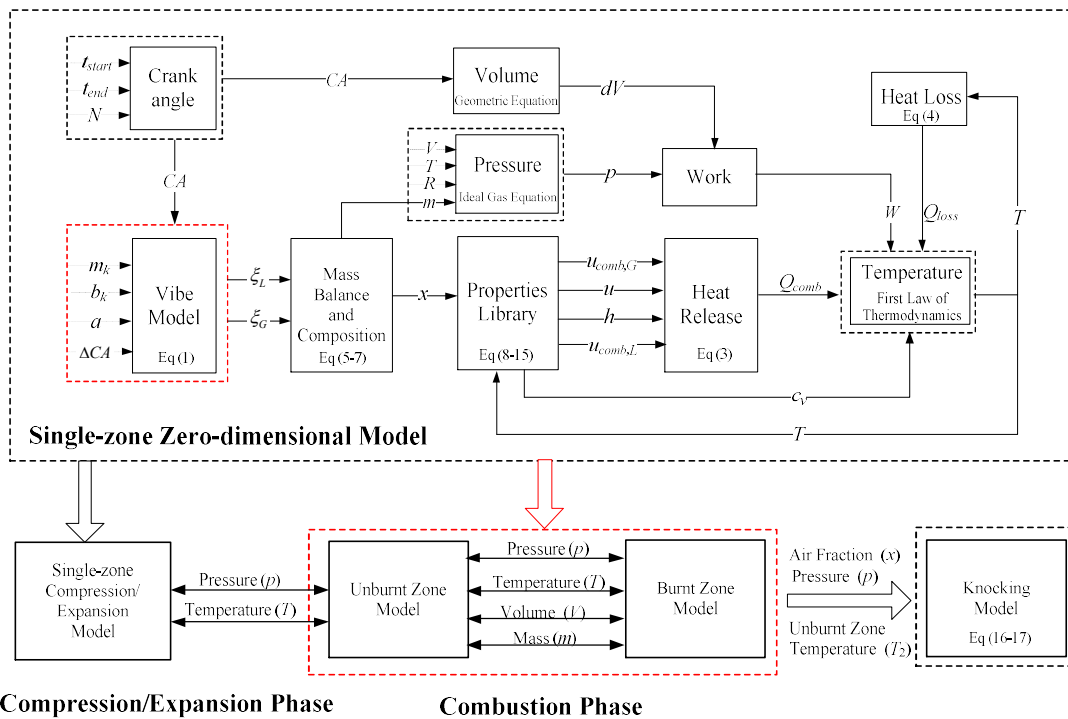
307 **2.2 Model Calculation Flowchart**

308 Figure 1 shows the calculation flowchart of the prediction model for evaluating the gaseous fuels
 309 interchangeability. A zero-dimensional model initially developed for diesel engines is extended with
 310 the consideration of the thermodynamic properties of gaseous fuels (NG, H₂) and is subsequently
 311 embedded into a two-zone knocking model proposed in previous work [22], which enables the prediction
 312 of the engine performance and the knocking resistance during the gaseous fuel interchangeability.

313 In the extended zero-dimensional model, the Vibe model is used to calculate the combustion rate,
 314 which is then employed for the determination of the mass balance and instantaneous composition fraction.
 315 The properties library is built on the assumption that the thermodynamic properties of the in-cylinder gas
 316 are functions of the composition and the temperature, which provides the combustion heat, the internal

317 energy, the enthalpy and the specific heat. The heat release rate is obtained by multiplying the combustion
 318 heat with fuel burning rate. The heat transfer coefficient in Heat Loss sub-model is estimated by using
 319 the Woschni formula. The in-cylinder temperature is calculated by employing the First Law of
 320 Thermodynamics.

321 The overall model consists of a two-zone module for representing the combustion phase and a single-
 322 zone module for modelling the compression and expansion phases. Both modules are developed based
 323 on the extended single-zone zero-dimensional model. The combustion submodel uses the multi-Vibe
 324 function to estimate the heat release rate. The in-cylinder parameters, including the air fraction, as well
 325 as the pressure and temperature of the unburnt zone are used to as input to calculate the knocking
 326 parameters.



327 **Compression/Expansion Phase** **Combustion Phase**
 328 Figure 1. Calculation flowchart of the prediction model for gaseous fuels interchangeability
 329

330 2.3 Model Setup

331 The geometric dimensions are the primary input of the proposed single-zone model. The engine
 332 rotational speed and the injected fuel mass need to be provided for determining the working conditions
 333 of the investigated internal combustion engines. The in-cylinder pressure and temperature at IVC are
 334 used to calculate the gas mass trapped in the cylinder at IVC. The charge efficiency is defined as the

335 mass ratio of the fresh air and the total trapped gas, which considers the existence of residual gas from
 336 previous working cycle. The employed fuels (liquid or gaseous) along with their compositions needs to
 337 be provided as input. For the combustion simulation of a direct-injection liquid fuel engine, the injection
 338 pressure is essential to evaluate the specific energy (e_f) caused by the injection pressure difference and
 339 the evaporation. In addition, the wall temperatures of the cylinder head, the cylinder liner and the piston
 340 top need to be set. In the *Combustion Model*, the Vibe parameters are required to calculate the heat release
 341 rate. The simulation period is set from the IVC to the exhaust valve opening (EVO), whilst the simulation
 342 step is set to be 0.5°CA . The crank angle is obtained from the time integration of the rotational speed
 343 assuming that the rotational speed remains constant. In addition, the fourth-order Runge-Kutta algorithm
 344 is used as the equations solver. Table 1 shows the input parameters of the single-zone model.

345

Table 1. Single-zone model input parameters

Geometric dimensions	Bore [m]	Fuel parameters	Composition
	Stroke [m]		Injection pressure [bar]
	Compression ratio [-]		
	Connecting rod length [m]	Combustion model	SOC, EOC [$^\circ\text{CA}$]
	IVC timing [$^\circ\text{CA}$]		b_i
	EVO timing [$^\circ\text{CA}$]		$m_{v, i}$
Working condition	Rotational speed [r/min]	Heat loss model	T_{head} [K]
	Injected fuel mass [kg/cycle/cylinder]		T_{liner} [K]
			T_{piston} [K]
Initial conditions	Pressure [bar]	Simulation parameters	Duration
	Temperature [K]		Step
	Charge efficiency [-]		Solver

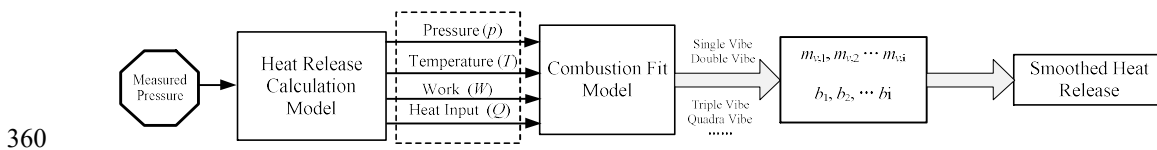
346 For the two-zone knocking prediction model, three more parameters (S_{mass} , λ_{ent} and S_{HH}) need to be
 347 provided as input besides the parameters shown in Table 1. The initial mass coefficient S_{mass} is defined
 348 as the ratio of the initial mass of the burnt zone and the overall cylinder zone, whereas λ_{ent} and S_{HH} are
 349 used to describe the mass and energy flow between the two gas phase zones. The entrainment factor λ_{ent}
 350 is introduced to account for the existence of the stoichiometric gas in the unburnt zone and the possibility
 351 that the excess air ratio entrained from the unburnt zone to the burnt zone could be more than or less than

352 1. The Heider–Holhbaum factor S_{HH} [22] is defined as the ratio of the stoichiometric gas flow leaving
 353 the burnt zone and the stoichiometric gas production rate.

354

355 2.4 Combustion Model Calibration

356 As the combustion characteristics varies with the engine working conditions, the combustion model
 357 needs to be calibrated before being used to predict the engine performance. In this study, heat release
 358 analysis is applied to determine the Vibe parameters, which are then used to simulate the fuel burning
 359 rate of single-fuel engines or multi-fuel engines.



360

361

Figure 2. Calculation flowchart of the combustion model calibration^[23]

362 Sui [23] proposed a way to calculate the heat release rate of diesel engines by applying an inverse
 363 in-cylinder model. Figure 2 presents the calculation flow of the combustion model calibration, which can
 364 be illustrated as follow.

- 365 1) The heat release rate can be obtained from the HRR analysis by using the measured in-cylinder
 366 pressure by employing heat release calculation model. Alternatively, Computational Fluid
 367 Dynamics (CFD) simulation tools can be used to estimate the heat release rate in case the measured
 368 pressure is not available.
- 369 2) For representing the obtained heat release rate with the combustion fit model, the number of the
 370 adopted Vibe functions needs to be determined according to the involved fuel types and the fuel
 371 injection method. In order to reduce the parameters number, the combustion start timing for all the
 372 gaseous fuels are considered to be the same. Then a curve fit method is applied to identify the Vibe
 373 parameters, including the start of combustion (*SOC*), the end of combustion (*EOC*), weight factors
 374 (b_i) and shape factors ($m_{v,i}$). a is set at 6.9078 to maintain a combustion efficiency of 99.9%.
- 375 3) The HRR obtained by employing the approach described above provides a smoother HRR than the
 376 one calculated from the in-cylinder pressure by using filtering. Thus, it is more suitable for the in-
 377 cylinder combustion modelling as the measurement fluctuations are eliminated [23].

378

379 3. Model Validation

380 As a number of issues may occur during the operation of gaseous fuel engines, such as the
 381 deteriorated engine dynamic behaviour as well as knocking or misfiring tendency, the fuel flexibility is
 382 proposed as a counter measure in gas or dual-fuel internal combustion engines like diesel-natural gas
 383 engines [38] and diesel-H₂-natural gas engines [39] As the proposed model is based on the calculation
 384 of the working medium thermodynamic properties and multi-Vibe combustion functions, it is practically
 385 capable of predicting the performance of all types of internal combustion engines with the developed
 386 properties library and the appropriate combustion model calibration. The model validation was carried
 387 out for four internal combustion engine cases, in specific, the MAN 20/27 diesel engine, the 2135 spark-
 388 ignited natural gas engine, the YC6K dual-fuel engine and the Lister Petter TR2 diesel-H₂-natural gas
 389 engine. The experimental data of the first three engines was obtained from engine tests [27], whilst that
 390 of the Lister Petter TR2 diesel-H₂-natural gas engine was taken from [41].

391

392 3.1 Diesel Engine

393 In this section, the model application to diesel engines is verified by comparing the derived results
 394 against experimental data from a MAN 20/27 diesel engine. The main characteristics of the MAN 20/27
 395 engine are shown in Table 2. ABDC represents after Bottom Dead Centre. BBDC represents before
 396 Bottom Dead Centre.

397 Table 2. Main characteristics of MAN 20/27 diesel engine ^[27]

Parameter	
Bore [mm]	200
Stroke [mm]	270
Nominal Engine Speed [rpm]	1000
Nominal power per cylinder [kW]	84
Compression Ratio	13.4:1
IVC [°CA, ABDC]	20
EVO [°CA, BBDC]	60

398 Figure 3(a) shows the comparison of the experimentally obtained data and the simulation results for
 399 the in-cylinder pressure of the MAN 20/27 diesel engine. As shown in Figure 3(a), the derived in-cylinder
 400 pressure sufficiently coincides with the measured one. In Figure 3(b), u_{comb} and $u_{comb, eff}$ represent the

401 combustion heat calculated by Eq (13) and Eq (15), respectively. The relative error between the u_{comb}
 402 and the LHV ranges from 1.31% to 2.81%, which implies that using the LHV in simulation tools would
 403 not provide a considerable error in the calculation of the heat release and engine power. With considering
 404 the influence of the liquid fuel evaporation, $u_{comb,eff}$ exhibits a sharp decrease of approximately
 405 $2.7 \cdot 10^6 \text{ J/kg}$ and a subsequent increase of $0.7 \cdot 10^6 \text{ J/kg}$, resulting in the largest relative deviation (from
 406 the LHV) of 8.03% at around 208°CA .

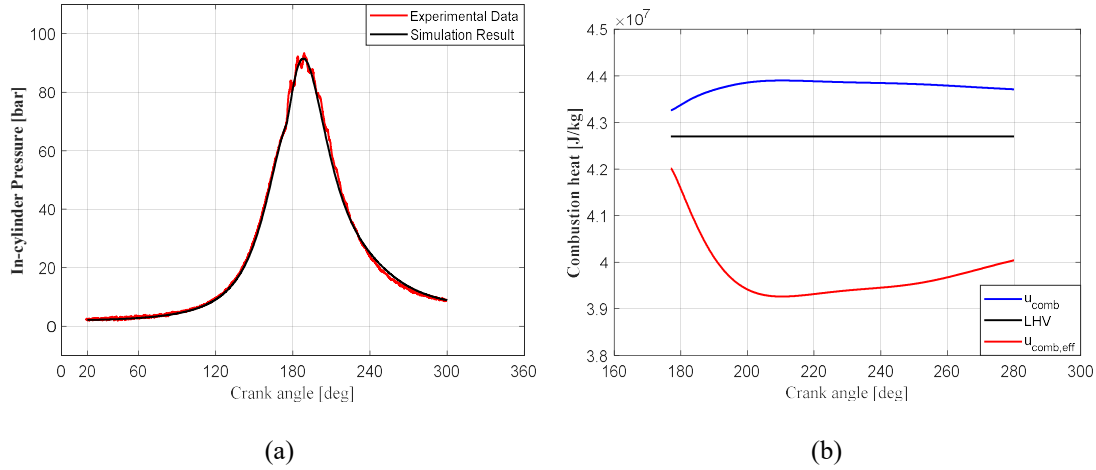


Figure 3. Simulation results and comparison with available experimental data for the MAN 20/27 diesel engine operating at its nominal power and speed; (a) the in-cylinder pressure; (b) the combustion heat.

407

408 3.2 Natural Gas Engine

409 Experimental data from the 2135 natural gas (NG) engine is used to verify the application of the
 410 proposed method on premixed SI engines operating with natural gas. The natural gas composition and
 411 the main characteristics of 2135 engine are provided in Table 3 and

412 Table 4.

413

Table 3. Natural gas composition

Composition	Fraction (%)
CH ₄	76.66
C ₂ H ₆	17.76
C ₃ H ₈	4.61
<i>n</i> -C ₄ H ₁₀	0.41
<i>i</i> -C ₄ H ₁₀	0.19

C_3H_{12}	0.06
N_2	0.31

414

415

Table 4. Main characteristics of 2135 natural gas engine

Parameter	
Bore [mm]	135
Stroke [mm]	140
Nominal Engine Speed [rpm]	1500
Nominal power per cylinder [kW]	11.92
Compression Ratio	11:1
IVC [$^{\circ}$ CA, ABDC]	48
EVO [$^{\circ}$ CA, BBDC]	48

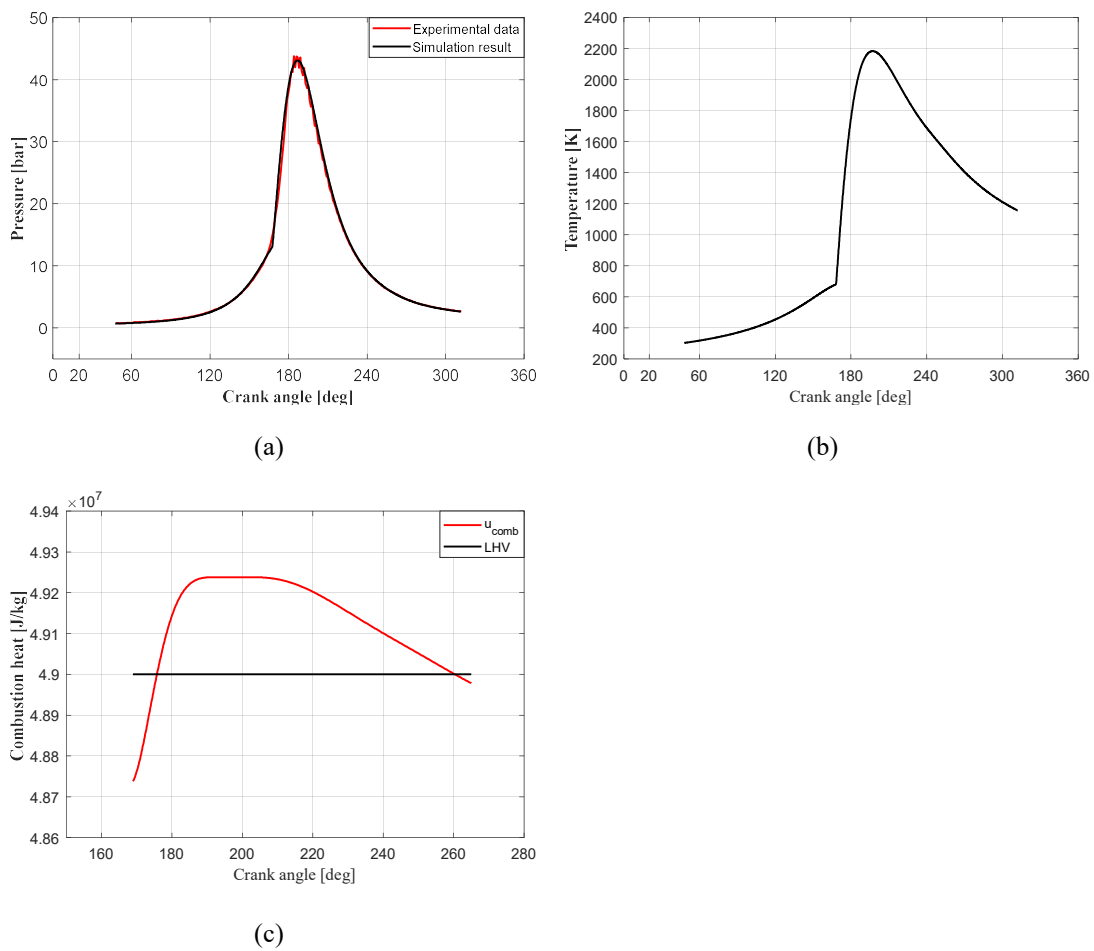


Figure 4. Simulation results and comparison with available experimental data for the 2135 natural

gas engine operating at its nominal power and speed; (a) the in-cylinder pressure; (b) the in-cylinder temperature; (c) the combustion heat.

416 As it can be inferred from Figure 4(a), the simulation results adequately coincide with the measured
417 in-cylinder pressure from the 2135 natural gas engine, which verifies the accuracy of the single-zone in-
418 cylinder model. Figure 4(b) and Figure 4(c) present the in-cylinder temperature and the combustion heat.
419 The combustion heat varies in a same trend with the in-cylinder temperature during the combustion
420 period as it is highly dependent on the temperature variation. In addition, u_{comb} is smaller than the LHV
421 during the periods of 169°CA to 177°CA and 252°CA to 265°CA due to the relatively lower temperature
422 of the in-cylinder working medium. The difference between the u_{comb} and the LHV of natural gas is quite
423 small (less than 0.55%) comparing to that of diesel fuel in Figure 3(b), which indicates that even a
424 constant LHV would not considerably affect the calculation accuracy.

425

426 3.3 Dual-fuel Engine

427 The YC6K dual fuel engine was converted from YC6K diesel engine by adding a natural gas supply
428 system and updating its Electronic Control Unit (ECU). It works in two different modes, the diesel mode
429 and dual-fuel mode. Diesel fuel with lower auto-ignition temperature serves as an ignition source for the
430 natural gas combustion. The diesel fuel contributes to 25.7% of the total energy release in dual-fuel mode
431 at the nominal working condition. The main characteristics of the YC6K dual-fuel engine are shown in
432 Table 5. Three Vibe functions are used to simulate the heat release corresponding to the diesel fuel
433 premixed combustion, the diesel fuel diffusion combustion and the natural gas combustion.

434

435 Table 5. Main characteristics of YC6K dual-fuel engine

Parameter	
Bore [mm]	129
Stroke [mm]	155
Nominal Engine Speed [rpm]	1800
Nominal power per cylinder [kW]	65
Compression Ratio	16.5:1
IVC [°CA, ABDC]	2

436

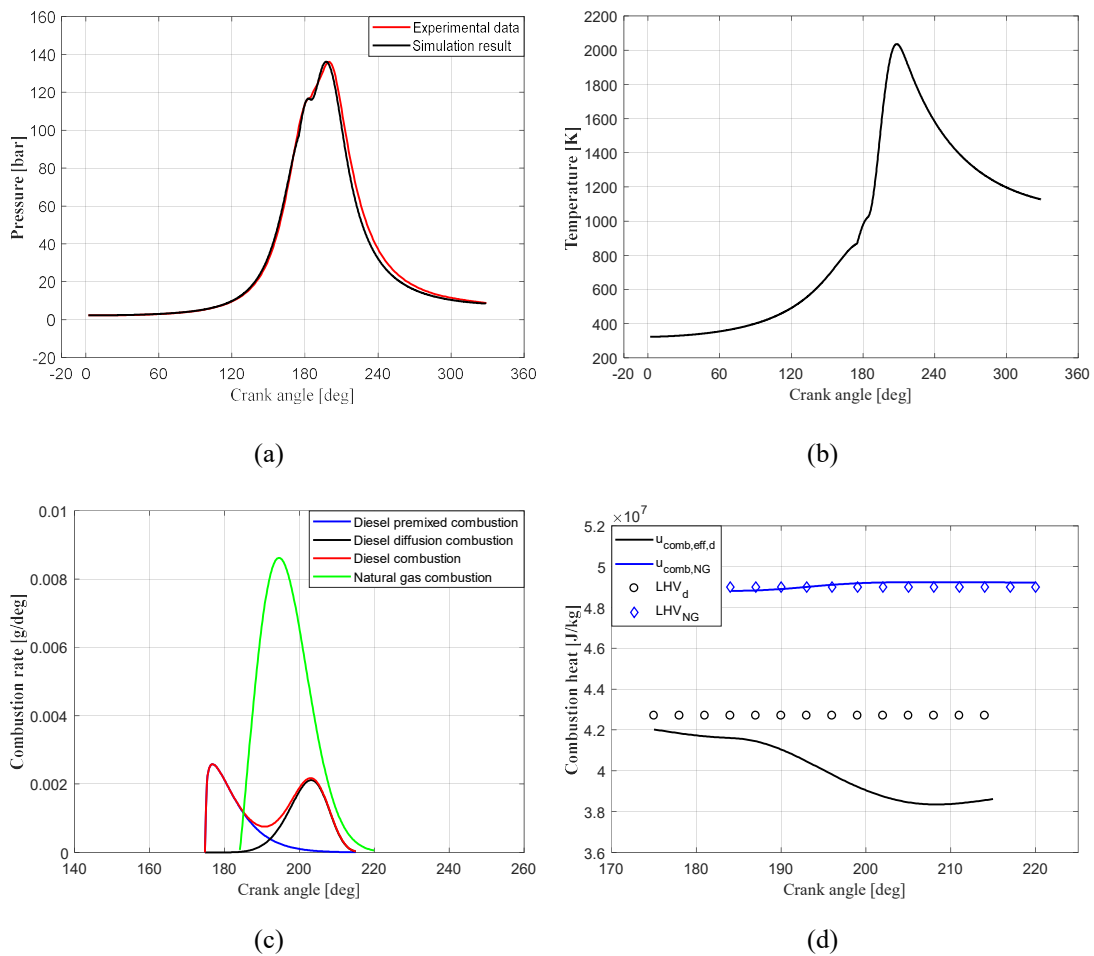


Figure 5. Simulation results and comparison with available experimental data for the YC6K dual fuel engine operating at its nominal power and speed; (a) in-cylinder pressure; (b) in-cylinder temperature; (c) combustion rates of diesel fuel and natural gas; (d) combustion heat of diesel fuel and natural gas.

437 Figure 5(a) presents the comparison of the derived in-cylinder pressure variation and the
 438 corresponding measured data. The measured pressure was obtained from an AVL combustion analyser,
 439 which smoothed the original pressure signal with its inbuilt algorithm. The simulation results are in
 440 sufficient coincidence with the measured pressure, whereas the predicted peak pressure crank angle is
 441 about 2.5°CA advanced in comparison with the experimental data. In this case, the dominant combustion
 442 phase is retarded after the top dead centre by delaying the diesel injection timing in order to decrease the
 443 average in-cylinder temperature for reducing the NO_x emissions. As can be inferred from Figure 5(b), the
 444 in-cylinder temperature is roughly controlled under 2000 K, which is the threshold that the thermal NO_x

445 begins to form rapidly [42].

446 Figure 5(c) shows the estimated total heat release rate, which consists of three parts corresponding
447 to the diesel fuel premixed combustion, the diesel fuel diffusion combustion and the natural gas premixed
448 combustion, respectively. One single Vibe function is used to characterize the combustion rate of natural
449 gas as it exhibits a premixed combustion behaviour [43]. In order to reduce the employed Vibe function
450 parameters number, the start and end timings of premixed combustion and diffusion combustion of the
451 diesel fuel are assumed to be the same. The start timing of the natural gas combustion is set at 8°CA after
452 that of the diesel fuel. Figure 5(d) shows the effective combustion heat variations of the diesel and the
453 natural gas fuels. The considerable drop (during 175°CA ~207°CA) caused by the liquid diesel fuel
454 evaporation can be easily spotted on the combustion heat of diesel fuel. By multiplying the combustion
455 heat by combustion rate, it can be inferred that the diesel fuel contributes 25.7% of the total energy
456 release.

457

458 **3.4 Tri-fuel Engine**

459 Lean burn technology is now widely used in NG engines to decrease the average in-cylinder
460 temperature for reducing the NO_x emissions. However, due to the slow flame speed of the NG mixture,
461 operational limitations of the engine settings (air-fuel ratio, injection/spark timing, etc.) must be imposed
462 for to ensure the smooth engine operation and low controlled emissions. In this respect, meeting the
463 existing and future emissions regulations without compromising the engine efficiency is a quite
464 challenging task [44], which depends on the engine type and application [45]. The enrichment of NG
465 with a fast-burning fuel, i.e. hydrogen, which has a laminar burning velocity sevenfold higher than that
466 of the NG and a low ignition energy limit, was reported to be an effective method to extend the lean
467 operation limit of the NG engines [41].

468 Abu-Jrai [41] carried out an experimental study by using a Lister Petter TR2 engine to study the
469 effect of tri-fuel (Ultra Low Sulfur Diesel (ULSD), H₂ and CH₄) operation on the combustion
470 characteristics. Engine tests using 20% (volumetric percentage of the total air inlet charge) H₂-CH₄
471 mixture injected in the inlet ports and direct injected ULSD were performed in three engine loads (25%,
472 50% and 75%) at a constant engine speed of 1500 rpm. The total air-fuel equivalence ratio was controlled
473 and was set at 1.4 for all the testing conditions. Part of the experimental data in [41] is used in this study
474 to verify the model applicability to the tri-fuel engines. The selected experimental data was measured at

475 1500 rpm and 75% load when the Lister Petter TR2 tri-fuel engine operated on two gaseous fuel-air
 476 mixtures (H50M50 and H75M25, respectively) and the ULSD. The constituents of H50M50 are 10% H₂,
 477 10% CH₄ and 80% air, whilst the H75M25 consists of 15% H₂, 5% CH₄ and 80% air. Table 6 shows the
 478 main characteristics of the Lister Petter TR2 tri-fuel engine.

479

Table 6. Main characteristics of Lister Petter TR2 engine^[41]

Parameter	
Bore [mm]	98.42
Stroke [mm]	101.6
Nominal Engine Speed [rpm]	1500
Nominal power per cylinder [kW]	6.05
Compression Ratio	15.5:1
IVC [°CA, ABDC]	32
EVO [°CA, BBDC]	76

480 Four Vibe functions are employed to calculate the HRR of the tri-fuel engine. This approach requires
 481 16 Vibe parameters to be determined as listed in Table 7. In order to reduce the Vibe parameters number,
 482 the weight factors estimated for the 20/27 diesel engine combustion (b_1 and b_2) are used to represent the
 483 premixed combustion stage and diffusion combustion stage of the ULSD. The shape factors estimated
 484 for the 20/27diesel engine combustion (m_1 and m_2) and the 2135 NG engine combustion (m_3) are used to
 485 simulate the heat release rate of ULSD and CH₄ in the tri-fuel engine combustion model. In addition, the
 486 H₂ and CH₄ are assumed to start combustion at the same timing and have the same combustion duration.
 487 The combustion start timings of the ULSD (SOC_1 and SOC_2) and the gaseous fuels (SOC_3 and SOC_4) can
 488 be deduced from the sharp increasing points on the measured HRR curves. The remaining three Vibe
 489 parameters m_4 , $\Delta\theta_1$ (also equal to $\Delta\theta_2$) and $\Delta\theta_3$ (also equal to $\Delta\theta_4$) are obtained by employing a curve
 490 fitting method. It is inferred from Table 7 that the gaseous fuels with higher H₂ content start combustion
 491 1°CA earlier, which is accompanied with shorter combustion durations for the diesel, CH₄ and H₂ fuels.

492

Table 7. Vibe parameters for HRR calculation in the tri-fuel engine model

	SOC_1	SOC_2	SOC_3	SOC_4	$\Delta\theta_1$	$\Delta\theta_2$	$\Delta\theta_3$	$\Delta\theta_4$
H50M50	176.5	176.5	180.5	180.5	22	22	10	10

H75M25	176.5	176.5	179.5	179.5	10	10	7.5	7.5
	m_1	m_2	m_3	m_4	b_1	b_2		
H50M50	0.4	3	1.5	1.0	0.88	0.12		
H75M25	0.4	3	1.5	1.0	0.88	0.12		

493

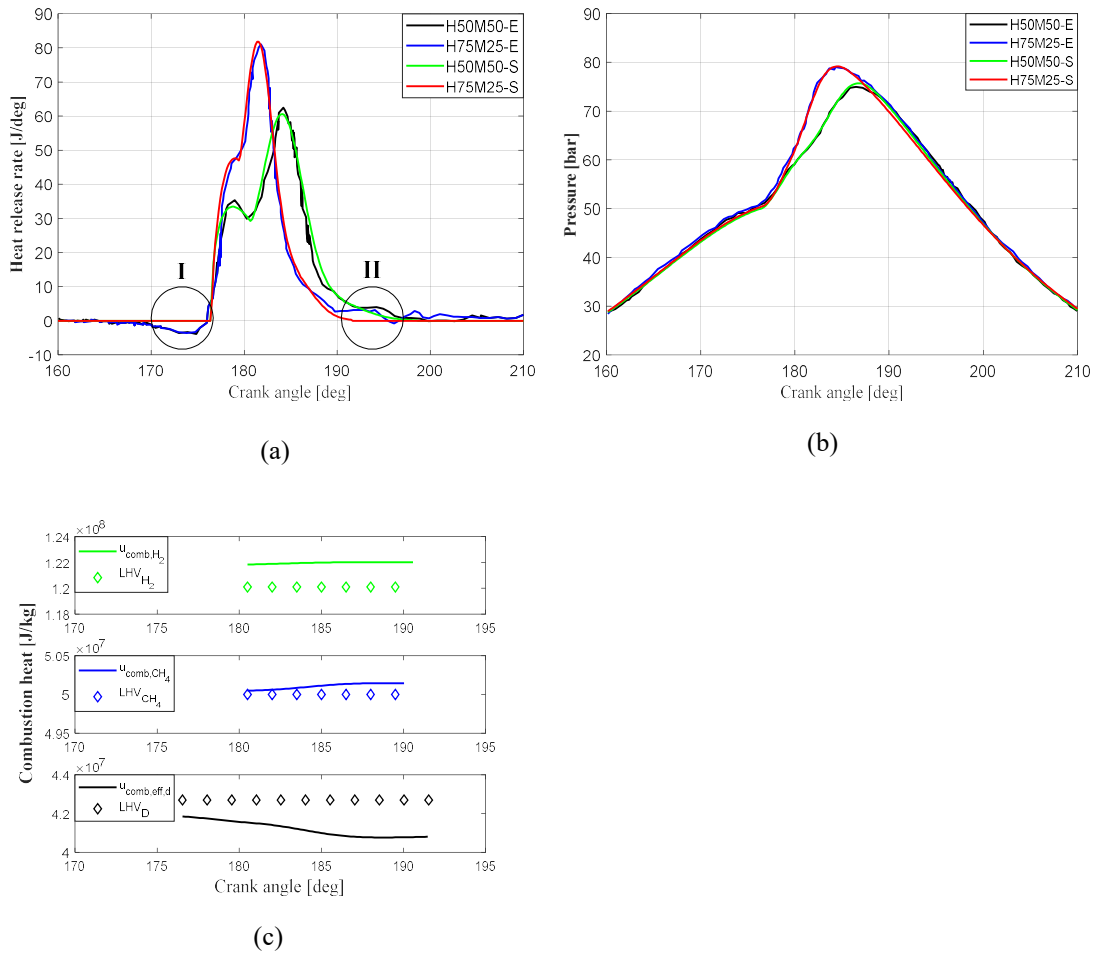


Figure 6. Simulation results and comparison with available experimental data for the Lister Petter TR2 tri-fuel engine operating at 1500 rpm and 75% load with H50M50 and H75M25 mixtures; (a) heat release rate; (b) in-cylinder pressure; (c) combustion heat.

494 Figure 6 shows the comparison of the simulation results with the respective experimental data for
 495 the tri-fuel engine with H50M50 and H75M25 fuel mixtures. In this figure, E represents the experimental
 496 data from literature [41], whilst S denotes the simulation results. The Vibe parameters in Table 7 were
 497 used to simulate the heat release rate of the tri-fuel engine, which adequately matches the experimental
 498 data during the dominant combustion phase except the zone I and Zone II parts, as shown in Figure 6(a).
 499 The deviation between the simulation and experimental data in Zone I is mainly attributed to the liquid

500 diesel fuel evaporation, which starts earlier than the combustion start, as an injection model is not used
501 in this study. The difference in Zone II is due to the heat loss that is included in the heat release calculated
502 from the experimentally obtained cylinder pressure, but not being considered for the calculation of the
503 net heat release in the developed model.

504 As can be deduced from Figure 6(b), the simulation results sufficiently agree with the measured in-
505 cylinder pressure for the investigated cases. Higher H₂ percentage tends to achieve a greater peak cylinder
506 pressure in an advanced crank angle than the respective ones in the case of a fuel mixture with a lower
507 H₂ percentage. This is attributed to the high hydrogen burning velocity, which result in a faster and
508 advanced heat release after the diesel fuel ignition, as shown in Figure 6 (a).

509 Figure 6(c) shows the combustion heat of the H₂, the CH₄ and the ULSD in comparison with their
510 LHVs. The combustion heat of H₂ is much higher than that of other fuels due to its extremely small molar
511 mass. The effective combustion heat of the liquid diesel fuel exhibits a decrease with a maximum relative
512 deviation of 8.03% compared to its LHV, whilst that of H₂, CH₄ slightly increase exhibiting a maximum
513 relative deviation of 1.67% and 0.3%, respectively compared to their LHVs.

514

515 **3.5 Quantitative Comparison**

516 Four in-cylinder parameters are chosen as criteria to verify the accuracy of the proposed single-zone
517 zero-dimensional model quantitatively, in specific, the Indicated Mean Effective Pressure (IMEP), the
518 pressure at EVO (p_{EO}), the peak pressure (p_{max}) and the corresponding crank angle (α_1). IMEP, p_{max} and
519 p_{EO} are related to the mechanical load and heat load of the cylinder to a certain extend. The comparison
520 of the simulation results and the experimental data is shown in Table 8. The error of α_1 is presented in the
521 form of absolute difference (°CA), whilst that of p_{max} and p_{EO} are indicated by the absolute error
522 percentage (%). In addition, p_{EO} for the tri-fuel engine case in Table 8 is actually the pressure value at
523 30°CA after top dead centre (ATDC), as Abu-Jrai [41] provided the in-cylinder pressure from 20°CA
524 before top dead centre (BTDC) to 30°CA ATDC instead of the complete in-cylinder process. The IMEP
525 comparison of the tri-fuel engine is not included in Table 8 due to the same reason. As can be seen from
526 Table 8, the relative errors of IMEP, p_{max} and p_{EO} are below 3%, whilst the absolute difference of the peak
527 pressure position are less than 3°CA. Thus, it can be inferred that the proposed in-cylinder single-zone
528 model is able to predict the performance of internal combustion engines operating with flexible fuels and
529 can be used with fidelity for the calculation presented in the next section.

531 Table 8. The quantitative comparison of p_{max} and p_{EO} between the simulation and the measurement

Parameters		IMEP (bar)	p_{EO} (bar)	p_{max} (bar)	α_1 (°CA ATDC)
Diesel engine	Simulation	11.96	8.88	91.54	8.1
	Measurement	12.02	8.93	93.33	9.7
	Error [% or °CA]	0.55	0.56	1.92	1.6
Natural gas engine	Simulation	4.65	2.44	44.22	4.0
	Measurement	4.76	2.51	44.31	7.0
	Error [% or °CA]	2.35	2.79	0.20	3.0
Dual-fuel engine	Simulation	21.00	8.52	136.00	16.8
	Measurement	21.39	8.76	136.10	19.0
	Error [% or °CA]	1.84	2.74	0.07	2.2
Tri-fuel engine (H50M50)	Simulation		29.19	75.71	6.8
	Measurement		29.05	74.96	6.5
	Error [% or °CA]		0.48	1.00	0.3
Tri-fuel engine (H75M25)	Simulation		29.47	79.17	4.5
	Measurement		29.43	79.02	4.3
	Error [% or °CA]		0.14	0.19	0.2

532

533 **4. Investigation on the Gaseous Fuel Interchangeability**

534 The Wobbe Index has been widely-used in practice as an unambiguous reference to assess the
535 interchangeability of gaseous fuels. According to the WI definition, the energy supplied to the engine
536 remains constant when the WI holds the same values for a constant engine air flow. Nevertheless, the WI
537 just provides a rough prediction of the involved fuel energy, which is not enough to evaluate the engine
538 performance with sufficient accuracy. In addition, inert gases like CO₂ and N₂ are often added to the raw
539 natural gas to maintain a constant WI in order to meet the fuel interchangeability requirements as well as
540 for avoiding controlling the variation of engine settings (i.e. spark timing or pilot fuel injection start).
541 The knocking resistance of a gaseous fuel-air mixture depends on its composition, the engine load, the

542 trapped air-fuel ratio and the temperature of the unburnt zone [10]. Thus, the addition of inert gases
 543 affects the engine knocking performance as the decreased LHV could reduce the in-cylinder temperature.

544 In this section, the developed engine model is employed to investigate the engine performance in
 545 cases where fuels (or gaseous fuels mixtures) with the same WI are used. In addition, the inert gas
 546 addition on engine knocking performance is investigated.

547

548 4.1 Engine Performance Prediction using fuels with the same Wobbe Index

549 In this section, the model as presented in the previous section is used to investigate the energy input
 550 and the engine power of the 2135 engine operating on three gaseous fuels with same WI. The composition
 551 and properties of the employed gaseous fuels were taken from [10], and shown in Table 9. As the fuel
 552 composition does not noticeably influence the combustion velocity [10], the heat release rate can be
 553 considered the same for the three investigated cases. The theoretical energy input of each cylinder is
 554 fixed at 3.8 kJ as it provides an approximate power of 11.92 kW. Then, the mass flow of the gaseous fuel
 555 and air can be calculated according to the fuel LHV considering that the air-fuel ratio is kept at its
 556 stoichiometric value as presented in Table 9. LPG represents liquefied petroleum gas.

557 Table 9. Fuel composition and properties of the investigated gaseous fuels ^[10]

	Volumetric fraction (%)				Heating value		WI	Stoichiometric air-fuel ratio
	CH ₄	C ₃ H ₈	CO ₂	N ₂	MJ/m ³	MJ/kg	MJ/m ³	[-]
Natural gas	81	2	3	14	31.68	38.11	39.47	12.62
LPG-CO ₂	-	54	46	-	50.33	23.95	39.47	8.59
LPG-N ₂	-	47	-	53	43.81	27.52	39.47	9.26

558 Table 10 shows the comparison of the theoretical values and the simulated results for the heat release
 559 and the engine power. The simulated energy input of the LPG-CO₂ mixture is 5.53% higher than its
 560 theoretical value, whilst the ones of the natural gas and the LPG-N₂ mixture are 5.26% and 1.05% lower
 561 than their theoretical values, respectively. Despite the 1.05% decrease from the theoretical energy input,
 562 the predicted engine power when the engine operates with LPG-N₂ mixture is 2.77% higher than its
 563 reference value. The derived engine power of the NG and the LPG-CO₂ mixture are 3.02 % lower and
 564 8.98 % higher than their theoretical values respectively, which are in accordance with the relative error

565 trend of their heat release.

566 Table 10. The energy input and the engine power with three gaseous fuels

	Heat release			Engine power		
	Theoretical value (kJ)	Calculated value (kJ)	Relative error (%)	Reference value (kW)	Calculated value (kW)	Relative error (%)
NG	3.80	3.60	-5.26	11.92	11.56	-3.02
LPG-CO ₂	3.80	4.01	5.53	11.92	12.99	8.98
LPG-N ₂	3.80	3.76	-1.05	11.92	12.25	2.77

567

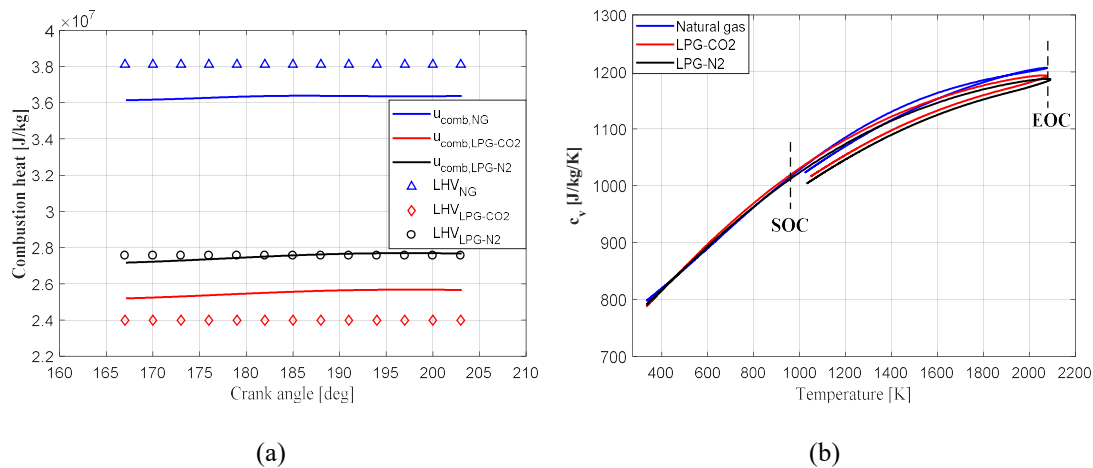


Figure 7. Simulation results for the 2135 engine operating at nominal conditions with natural gas, LPG-CO₂ mixture and LPG-N₂ mixture; (a) combustion heat versus crank angle; (b) specific heat of the in-cylinder gases versus in-cylinder temperature.

568 Figure 7(a) presents the combustion heat variation with the crank angle for the three investigated
 569 gaseous fuels. As deduced from Figure 7(a), the combustion heat of the LPG-N₂ mixture roughly equals
 570 to its LHV, leading to the smallest relative error for the heat release and the engine power when the 2135
 571 engine operates with LPG-N₂ mixture. The average combustion heat of the NG is about 5.3% lower than
 572 its LHV, whilst the average combustion heat of the LPG-CO₂ mixture is approximately 5.5% higher than
 573 its LHV, which matches to the engine power variation trend.
 574 Figure 7(b) shows the specific heats at constant volume of the in-cylinder gases as functions of the in-
 575 cylinder temperature. The high content of the H₂O vapour in the NG combustion products results in a

576 higher specific heat than that of the other mixtures during the combustion phase. With regard to the
 577 comparison between the LPG-CO₂ and the LPG-N₂ mixtures, the greater amount of CO₂ that has a higher
 578 specific heat results in a greater specific heat of the LPG-CO₂ mixture (the latter is higher in comparison
 579 with that of the LPG-N₂ mixture).

580

581 4.2 Influence of Inert Gas Addition on Knocking Performance

582 In this section, the influence of the CO₂ and N₂ addition on the knocking performance of the 2135
 583 engine operating on natural gas is investigated. The Adu Dhabi natural gas [46], which has one of the
 584 lowest knock resistances because of its high ethane content, is used as the baseline gaseous fuel herein,
 585 whilst the volumetric addition of CO₂ and N₂ is set to be 5%, 10%, 15% and 20%, as shown in Table 11.
 586 Motor Octane Numbers (MON) of the fuel-inert gas mixtures are obtained according to the equation for
 587 MON and MN [46, 47]. The fuel consumption rate in each case is calculated referring to the fact that the
 588 volumetric flow of the gaseous fuel is inversely proportional to the square root of its density for a
 589 naturally aspirated premixed engine.

590 Table 11. Composition and MON of natural gas with different inert gas additions

Volumetric Fraction (%)	Natural gas	CO ₂ addition				N ₂ addition			
		+ 5%	+ 10%	+ 15%	+20%	+ 5%	+ 10%	+ 15%	20%
CH ₄	82	77.9	73.8	69.7	65.6	77.9	73.8	69.7	65.6
C ₂ H ₆	15.8	15.01	14.22	13.43	12.64	15.01	14.22	13.43	12.64
C ₃ H ₈	2.2	2.09	1.98	1.87	1.76	2.09	1.98	1.87	1.76
CO ₂	0	5	10	15	20	0	0	0	0
N ₂	0	0	0	0	0	5	5	15	20
MON	119.2	122.4	125.7	128.9	132.2	120.3	121.4	122.5	123.6

591

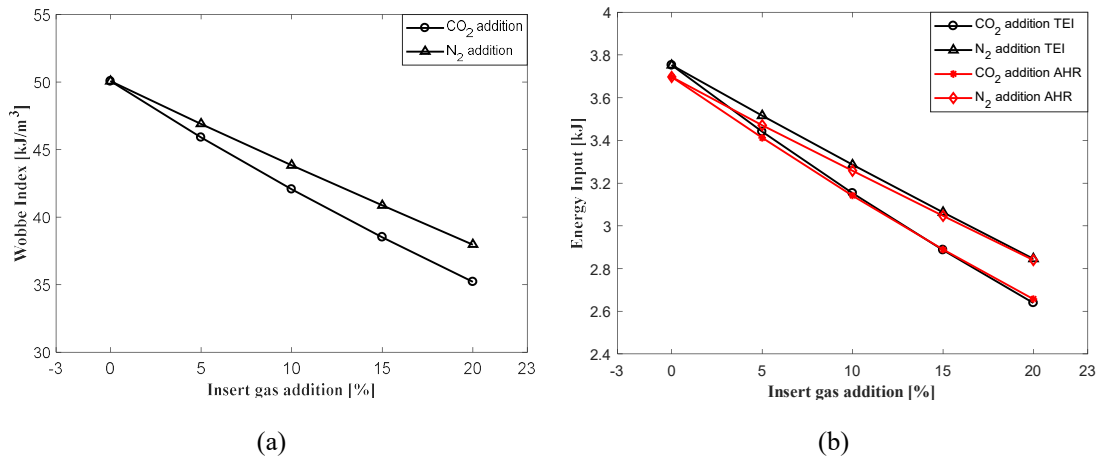


Figure 8. Simulation results for the 2135 engine operating on natural gas with 5%, 10%, 15% and 20% addition of CO₂ and N₂; (a) Wobbe Index variation; (b) Energy input variation.

592 Figure 8(a) shows the Wobbe Index variation of the natural gas with 0%, 5%, 10%, 15% and 20%
 593 CO₂ and N₂ additions, respectively. As shown in Figure 8(a), in both cases the Wobbe Index decreases
 594 almost linearly with the increase of the CO₂ and N₂ addition. CO₂ proves to be more effective than N₂ in the
 595 Wobbe Index reduction as the CO₂ density is about 1.6 times the N₂ density under standard conditions
 596 ($p=101.325$ kPa, $T=273.15$ K).

597 In Figure 8(b), the derived (for an engine cylinder) Theoretical Energy Input (TEI) and the
 598 Accumulated Heat Release (AHR) variations with different inert gas addition volumetric percentages are
 599 presented. The TEI is calculated by the LHV and the supplied fuel mass, whilst the AHR is obtained from
 600 the simulation model. As the input of the chemical fuel energy is directly proportional to the value of the
 601 Wobbe Index for a naturally aspirated premixed engine, both TEI values with the CO₂ and N₂ additions
 602 appear to decrease in the same trend with the WI variation shown in Figure 8(a). In addition, the AHR
 603 values for all cases are smaller than the corresponding TEI values (except for the case of 20%(vol) CO₂
 604 addition), as they are calculated by the internal energy difference of the combustion reactants and
 605 products as function of the average in-cylinder gas temperature, which is much greater than the
 606 temperature in standard conditions.

607 As the detection of knocking onset in NG engines might be sensitive to the simulation step, various
 608 simulation step values (0.5°CA, 0.2°CA and 0.1°CA) were tested to investigate the effects of the
 609 simulation step on the knocking onset. However, the knocking onset remains at 15°CA ATDC, which
 610 indicates that the investigated simulation step values did not affect considerably the knocking onset. This
 611 is attributed to the fact that the knocking prediction is based on an empirical knocking formula and a

612 two-zone model, which is relatively simplified and does not rely much on the simulation step. Thus, the
613 following simulation works for the knocking prediction are performed with a fixed simulation step of
614 0.5 °CA.

615 Figure 9(a) shows the natural induction time integral with varying inert CO₂ and N₂ addition rates,
616 which indicates the occurrence of knocking phenomenon when it reaches unity. As shown in Figure 9(a),
617 the addition of CO₂ causes a significant decrease of the final value of the natural induction time integral,
618 whilst the N₂ addition results in a relatively smaller decrease of the natural induction time. Figure 9(b)
619 shows the knocking index, which provides the relative knocking probability with different inert gases
620 addition rates. The knocking index with 0% inert gas addition is set to 100 as it represents the baseline
621 condition. It can be inferred from Figure 9(b) that both the CO₂ addition and the N₂ addition can reduce
622 the knocking probability of the natural gas engine with different levels. The CO₂ addition seems to be
623 more effective than N₂ in eliminating the knocking phenomenon, as the knocking index decreases to zero
624 with a 16% CO₂ addition, whilst the knocking index with 20% N₂ addition remains at 17.

625 Figure 9(c) and Figure 9(d) show the knocking position and knocking intensity with different inert
626 gases (CO₂ and N₂) addition rates. These two parameters are presented in the form of the crank angle
627 after the cylinder top dead centre (ATDC) and the mass fraction of the unburnt fuel in unburnt zone when
628 the knocking phenomenon happens, respectively. The knocking position is retarded by 19°CA with
629 15%(vol) CO₂ addition. For a CO₂ addition over 16% (vol), knocking does not occur, therefore, knocking
630 position is not shown in Figure 9 (c). The knocking intensity decreases from 21.5% to 0% when the CO₂
631 addition increases from 0% to 16%. The N₂ addition from 5% to 20% retards the knocking position by
632 10.5°CA and decreases the knocking intensity by 12%.

633

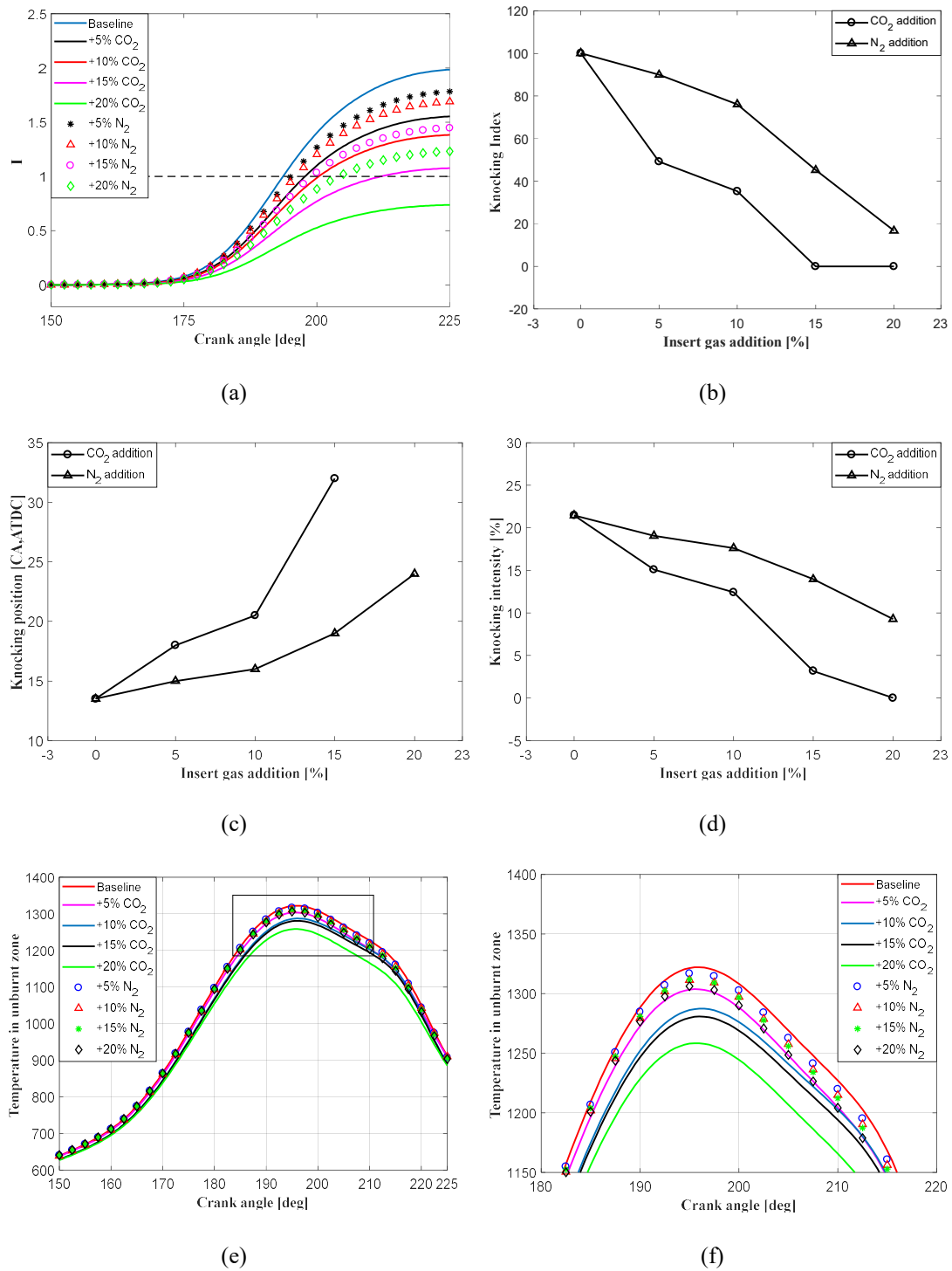


Figure 9. Simulation results for the 2135 engine operating on natural gas with 5%, 10%, 15% and 20% addition of CO₂ and N₂; (a) natural induction time integration; (b) knocking index; (c) knocking position; (d) knocking intensity; (e) the average temperature in unburnt zone (original); (f) the average temperature in unburnt zone (zoom in).

634 Figure 9(e) and Figure 9(f) present the gas temperatures of the unburnt zone with different inert gas
 635 addition rates. The unburnt zone gas temperature reduces with the increase of the CO₂ and N₂ addition

636 rates, which results in the knocking probability reduction according to Eq (17). As CO₂ has higher
637 specific heat capacity and higher density than the N₂ ($\rho_{CO_2} = 1.977 \text{ kg/m}^3$, $\rho_{N_2} = 1.25 \text{ kg/m}^3$ at standard
638 conditions), the CO₂ addition more significantly reduces the unburnt zone temperature, resulting in better
639 knocking resistance.

640

641 5. Conclusions

642 This study proposed an extended zero-dimensional model capable of simulating the multi-fuel
643 internal combustion engines, which employs the calculation of the thermodynamic properties of multiple
644 fuel mixtures and their combustion products. Subsequently, the extended model was used to investigate
645 the interchangeability between gaseous fuels with same WI and the influence of the inert gases (CO₂ and
646 N₂) addition on the engine knocking resistance. The main findings of this study are summarised as follow.

- 647 1. The maximum error between the simulation results and the respective experimental data was in the
648 range of 3% (obtained for the prediction of the in-cylinder pressure) implying that the extended
649 model shows adequate accuracy in predicting the operating parameters of the investigated internal
650 combustion engines operating on single or multiple fuels, including diesel engines, natural gas spark-
651 ignited engines, dual fuel engines and tri-fuel engines.
- 652 2. In terms of the energy input and the engine power, the relative errors between the WI estimation and
653 the results obtained by the developed model can be as high as 5.53% and 8.98% respectively, which
654 implies that simulation tools of adequate accuracy must be used for the engine performance
655 prediction with fuels interchangeability to avoid possible errors occurring by considering the WI.
- 656 3. The knocking probability of the 2135 NG engine is eliminated when the CO₂ addition rate increases
657 to around 16%, which is accompanied with a delay of 19°CA for the knocking crank angle and a
658 decrease of 21.5% for the knocking intensity.
- 659 4. The N₂ addition from 5% to 20%, it retards the knocking position by 10.5°CA and decreases the
660 knocking intensity by 12%.
- 661 5. Based on the preceding points, it is concluded that the CO₂ addition is more effective than the N₂
662 addition for suppressing the engine knocking in the investigated natural gas engine.

663 The proposed model extension in this paper is based on thermodynamic properties estimation and
664 multi-Vibe functions, which are practically applicable to the zero-dimensional model development of all

665 types of internal combustion engines, especially for those operating with flexible fuels. Compared to the
666 traditional WI method, it provides more accurate and detailed information of the fuel interchangeability
667 influence on engine performance and knocking resistance and therefore it is expected that the proposed
668 model will be a useful tool that can be used in the analysis of multi-fuel engines.

669

670 **Acknowledgements**

671 This project partly is financially supported by ‘International Science & Technology Cooperation
672 Program of China’, 2014DFG72360; National Key R&D Program of China, 2016YFC0205203. The
673 second author greatly acknowledges the financial support by the MSRC sponsors DNV GL and RCCL.

674

675 **Abbreviations**

ABDC	After Bottom Dead Centre
AGA	American Gas Association
AHR	Accumulated Heat Release
ATDC	After Top Dead Centre
BBDC	Before Bottom Dead Centre
BTDC	Before Top Dead Centre
CA	Crank Angle
CFD	Computational Fluid Dynamics
DFT	Density Functional Theory
ECU	Electronic Control Unit
EVO	Exhaust Valve Open
EOC	End of Combustion
HRR	Heat Release Rate
HV	Heating Value
IMEP	Indicated Mean Effective Pressure
IVC	Intake Valve Close
LHV	Lower Heating Value
LPG	Liquefied Petroleum Gas
MN	Methane Number
MON	Motor Octane Number
NG	Natural Gas
ON	Octane Number
PM	Particulate Matter
SI	Spark-Ignited
SOC	Start of Combustion

TDC	Top Dead Centre
TEI	Theoretical Energy Input
THC	Total Hydrocarbons
ULSD	Ultra Low Sulphur Diesel
WI	Wobbe Index

676

677 **Symbols**

$A_{wall,i}$	the heat transfer surface area, [m ²]
Q_{comb}	the total heat release, [J]
Q_{loss}	the total heat loss, [J]
T	the average in-cylinder temperature, [K]
T_{norm}	the reference temperature for the thermodynamic property fitting equations, [K]
T_{shift}	the shift temperature for the thermodynamic property fitting equations, [K]
T_2	the average temperature of the unburnt zone, [K]
$T_{wall,i}$	the average wall temperature, [K]
a	the coefficient related to the combustion efficiency in Vibe function, [-]
a_k	the fitting coefficient for the specific heat at constant pressure, [-]
$\alpha_{g \rightarrow w}$	the instantaneous heat transfer coefficient from the in-cylinder gas to the walls, [J/K/m ²]
b_i	the weigh factor of each fuel, [-]
c_p	the specific heat at constant pressure, [J/kg/K]
c_v	the specific heat at constant volume, [J/kg/K]
e_f	the specific energy variation caused by the liquid fuel injection and evaporation, [J/kg]
f_c	the property parameter (c_v , h and u) for each basic species, [-]
h	the specific enthalpy, [J/kg]
$h_{f,liquid}^{in+}$	the specific enthalpy of the liquid fuel, [J/kg]
h_j^{ref}	the specific enthalpy at standard condition, [J/kg]
$\dot{m}_{f,in}$	the diesel flow rate, [kg/s]
m_0	the mass of the in-cylinder gas mixture at IVC, [kg]
m_i	the injected fuel mass of each fuel, [kg]
m_v	the shape factor in Vibe function, [-]
p	the average in-cylinder pressure, [pa]
t	the elapsed time from the start of the compression process in unburnt zone, [s]
t_i	the time of auto-ignition timing, [s]
τ	the natural induction time, [ms]
τ_v	the normalized combustion time, [-]
u	the specific energy, [J/kg]
u_a	the specific internal energy of air, [J/kg]
u_{comb}	the combustion heat, [J/kg]

$u_{comb,G}$	the combustion heat of the gaseous fuel, [J/kg]
$u_{comb,L}$	the combustion heat of the liquid fuel, [J/kg]
$u_{comb,eff}$	the effective combustion heat, [J/kg]
u_f	the specific internal energy of fuel, [J/kg]
u_j^{ref}	the specific internal energy at standard condition, [J/kg]
u_{sg}	the specific internal energy of stoichiometric gas, [J/kg]
x_a	the air mass fraction, [%]
x_b	the burnt fuel fraction, [%]
x_f	the fuel mass fraction, [%]
x_{sg}	the mass fraction of the combustion products, [%]
x_c	the mass fraction of the considered mixtures constituents, [%]
x_e	the mass fraction of air, gaseous fuel and stoichiometric gas, [%]
x_0	the air mass fraction at IVC, [%]
x_1	the mass fraction of the air-fuel mixture at IVC in premixed engines, [%]
σ	the stoichiometric ratio, [-]
ζ	the fuel burning rate, [kg/s]
ζ_G	the fuel burning rate of the gaseous fuel, [kg/s]
ζ_L	the fuel burning rate of the liquid fuel, [kg/s]
θ	the normalized temperature, [-]
θ_{ref}	the normalized reference temperature, [-]

678

679 References

- 680 1. Mavrelou, C. and G. Theotokatos, *Numerical investigation of a premixed combustion large*
681 *marine two-stroke dual fuel engine for optimising engine settings via parametric runs.*
682 *Energy Conversion and Management*, 2018. **160**: p. 48-59.
- 683 2. Barati, M.R., et al., *Comprehensive exergy analysis of a gas engine-equipped anaerobic*
684 *digestion plant producing electricity and biofertilizer from organic fraction of municipal*
685 *solid waste.* *Energy Conversion and Management*, 2017. **151**: p. 753-763.
- 686 3. Thomson, H., J.J. Corbett, and J.J. Winebrake, *Natural gas as a marine fuel.* *Energy Policy*,
687 2015. **87**: p. 153-167.
- 688 4. Ghaderi, M., et al., *Design, fabrication and characterization of infrared LVOFs for*
689 *measuring gas composition.* *Journal of Micromechanics and Microengineering*, 2014. **24**(8):
690 p. 084001.
- 691 5. Kakae, A.-H., A. Paykani, and M. Ghajar, *The influence of fuel composition on the*
692 *combustion and emission characteristics of natural gas fueled engines.* *Renewable and*
693 *Sustainable Energy Reviews*, 2014. **38**: p. 64-78.
- 694 6. Jahanian, O. and S. Jazayeri, *A comprehensive numerical study on effects of natural gas*
695 *composition on the operation of an HCCI engine.* *Oil & Gas Science and Technology—Revue*
696 *d'IFP Energies nouvelles*, 2012. **67**(3): p. 503-515.
- 697 7. Ortíz, J., *Fundamentos de la intercambiabilidad del Gas Natural.* *Ciencia*, 2014: p. 6-15.
- 698 8. Halchuk-Harrington, R. and R. Wilson, *AGA Bulletin #36 and Weaver Interchangeability*
699 *Methods: Yesterday's Research and Today's Challenges*, in *Operating Section Proceeding -*
700 *Gas Association.* 2006, American Gas Association: Paramus, N.J. p. 802-823.
- 701 9. Eichmann, S.C., et al., *Determination of gas composition in a biogas plant using a Raman-*
702 *based sensor system.* *Measurement Science and Technology*, 2014. **25**(7): p. 075503.
- 703 10. Klimstra, J., *Interchangeability of Gaseous Fuels—the Importance of the WOBBE-INDEX.*

- 1986, SAE Technical Paper.
- 705 11. Karavalakis, G., et al., *The effect of natural gas composition on the regulated emissions,*
706 *gaseous toxic pollutants, and ultrafine particle number emissions from a refuse hauler*
707 *vehicle.* Energy, 2013. **50**: p. 280-291.
 - 708 12. Cardona, C.A. and A.A. Amell, *Laminar burning velocity and interchangeability analysis of*
709 *biogas/C₃H₈/H₂ with normal and oxygen-enriched air.* International Journal of Hydrogen
710 Energy, 2013. **38**(19): p. 7994-8001.
 - 711 13. Honus, S., S. Kumagai, and T. Yoshioka, *Replacing conventional fuels in USA, Europe, and*
712 *UK with plastic pyrolysis gases—Part I: Experiments and graphical interchangeability*
713 *methods.* Energy Conversion and Management, 2016. **126**: p. 1118-1127.
 - 714 14. Honus, S., S. Kumagai, and T. Yoshioka, *Replacing conventional fuels in USA, Europe, and*
715 *UK with plastic pyrolysis gases—Part II: Multi-index interchangeability methods.* Energy
716 Conversion and Management, 2016. **126**: p. 1128-1145.
 - 717 15. Baldi, F., G. Theotokatos, and K. Andersson, *Development of a combined mean value—zero*
718 *dimensional model and application for a large marine four-stroke Diesel engine simulation.*
719 Applied Energy, 2015. **154**: p. 402-415.
 - 720 16. Ding, Y., D. Stapersma, and H. Grimmelius, *Using parametrized finite combustion stage*
721 *models to characterize combustion in diesel engines.* Energy & Fuels, 2012. **26**(12): p. 7099-
722 7106.
 - 723 17. Maurya, R.K. and P. Mishra, *Parametric investigation on combustion and emissions*
724 *characteristics of a dual fuel (natural gas port injection and diesel pilot injection) engine*
725 *using 0-D SRM and 3D CFD approach.* Fuel, 2017. **210**: p. 900-913.
 - 726 18. Demir, U., et al., *Evaluation of zero dimensional codes in simulating IC engines using*
727 *primary reference fuel.* Applied Thermal Engineering, 2015. **76**: p. 18-24.
 - 728 19. Xu, S., et al., *A phenomenological combustion analysis of a dual-fuel natural-gas diesel*
729 *engine.* Proceedings of the Institution of Mechanical Engineers, Part D: Journal of
730 Automobile Engineering, 2017. **231**(1): p. 66-83.
 - 731 20. Kaprielian, L., et al., *Multi-zone quasi-dimensional combustion models for Spark-Ignition*
732 *engines.* 2013, SAE Technical Paper.
 - 733 21. Zhen, X., et al., *The engine knock analysis—an overview.* Applied Energy, 2012. **92**: p. 628-
734 636.
 - 735 22. Xiang, L., E. Song, and Y. Ding, *A Two-Zone Combustion Model for Knocking Prediction of*
736 *Marine Natural Gas SI Engines.* Energies, 2018. **11**(3): p. 561.
 - 737 23. Sui, C., et al., *Mean value modelling of diesel engine combustion based on parameterized*
738 *finite stage cylinder process.* Ocean Engineering, 2017. **136**: p. 218-232.
 - 739 24. Bulfin, B., et al., *Thermodynamics of CeO₂ thermochemical fuel production.* Energy & Fuels,
740 2015. **29**(2): p. 1001-1009.
 - 741 25. Hutter, R., et al., *Low-Load Limit in a Diesel-Ignited Gas Engine.* Energies, 2017. **10**(10): p.
742 1450.
 - 743 26. Ding, Y., et al., *Thermodynamics Properties Modeling of the Diesel Fuel and In-cylinder Gas*
744 *for Diesel Engines to Combustion Investigation.* Energy & Fuels, 2018.
 - 745 27. Ding, Y., *Characterising combustion in diesel engines,* in TU Delft. 2011.
 - 746 28. Neto, A., et al., *Thermodynamic analysis of fuels in gas phase: ethanol, gasoline and*
747 *ethanol—gasoline predicted by DFT method.* Journal of molecular modeling, 2015. **21**(10):
748 p. 267.
 - 749 29. Li, W., et al., *Experimental and theoretical analysis of effects of equivalence ratio on mixture*
750 *properties, combustion, thermal efficiency and exhaust emissions of a pilot-ignited NG*
751 *engine at low loads.* Fuel, 2016. **171**: p. 125-135.
 - 752 30. Merker, G.P., et al., *Simulating Combustion: Simulation of combustion and pollutant*
753 *formation for engine-development.* Vol. 7. 2005: Springer Science & Business Media.
 - 754 31. Ghojel, J.I., *Review of the development and applications of the Wiebe function: a tribute to*
755 *the contribution of Ivan Wiebe to engine research.* International Journal of Engine Research,
756 2010. **11**(4): p. 297-312.
 - 757 32. Woschni, G., *A universally applicable equation for the instantaneous heat transfer coefficient*
758 *in the internal combustion engine.* 1967, SAE Technical paper.
 - 759 33. Yaws, C.L., *Handbook of Thermodynamic Diagrams, Volume 3.* Vol. 4. 1986, USA: Gulf
760 Publication Company.
 - 761 34. Borman, G.L. and K.W. Ragland, *Combustion engineering.* 1998: McGraw-Hill

- 762 Science/Engineering/Math.
- 763 35. Wang, Z., et al., *Relationship between super-knock and pre-ignition*. International Journal of
764 Engine Research, 2015. **16**(2): p. 166-180.
- 765 36. Qi, Y., et al., *Effects of thermodynamic conditions on the end gas combustion mode associated*
766 *with engine knock*. Combustion and Flame, 2015. **162**(11): p. 4119-4128.
- 767 37. Livengood, J. and P. Wu. *Correlation of autoignition phenomena in internal combustion*
768 *engines and rapid compression machines*. in *Symposium (international) on combustion*. 1955.
769 Elsevier.
- 770 38. Kakaee, A.-H., P. Rahnama, and A. Paykani, *Influence of fuel composition on combustion*
771 *and emissions characteristics of natural gas/diesel RCCI engine*. Journal of natural gas
772 science and engineering, 2015. **25**: p. 58-65.
- 773 39. Mansor, M.R.A., M.M. Abbood, and T.I. Mohamad, *The influence of varying hydrogen-*
774 *methane-diesel mixture ratio on the combustion characteristics and emissions of a direct*
775 *injection diesel engine*. Fuel, 2017. **190**: p. 281-291.
- 776 40. !!! INVALID CITATION !!! [38, 39].
- 777 41. Abu-Jrai, A.M., H. Ala'a, and A.O. Hasan, *Combustion, performance, and selective catalytic*
778 *reduction of NOx for a diesel engine operated with combined tri fuel (H₂, CH₄, and*
779 *conventional diesel)*. Energy, 2017. **119**: p. 901-910.
- 780 42. Stiesch, G., *Modeling engine spray and combustion processes*. Vol. Heat & Mass Transfer.
781 2013: Springer Science & Business Media.
- 782 43. Ghojel, J., *Review of the development and applications of the Wiebe function: a tribute to the*
783 *contribution of Ivan Wiebe to engine research*. International Journal of Engine Research,
784 2010. **11**(4): p. 297-312.
- 785 44. Yan, F., L. Xu, and Y. Wang, *Application of hydrogen enriched natural gas in spark ignition*
786 *IC engines: from fundamental fuel properties to engine performances and emissions*.
787 Renewable and Sustainable Energy Reviews, 2017.
- 788 45. Valladolid, P.G., et al., *Impact of diesel pilot distribution on the ignition process of a dual*
789 *fuel medium speed marine engine*. Energy Conversion and Management, 2017. **149**: p. 192-
790 205.
- 791 46. Brecq, G., et al., *Knock prevention of CHP engines by addition of N₂ and CO₂ to the natural*
792 *gas fuel*. Applied thermal engineering, 2003. **23**(11): p. 1359-1371.
- 793 47. Kubesh, J., S.R. King, and W.E. Liss, *Effect of gas composition on octane number of natural*
794 *gas fuels*. SAE transactions, 1993. **101**: p. 1862-1862.

795